Journal of Quantitative Spectroscopy & Radiative Transfer 112 (2011) 1394–1401

Contents lists available at ScienceDirect

Journal of Quantitative Spectroscopy & Radiative Transfer

journal homepage: www.elsevier.com/locate/jqsrt

Notes

An improved wavelength selection scheme for Monte Carlo solvers applied to hypersonic plasmas

Andrew Feldick [a], Michael F. Modest [b,*]

[a] Department of Mechanical and Nuclear Engineering, The Pennsylvania State University, University Park, PA 16802, USA
[b] School of Engineering, University of California Merced, Merced, CA 95340, USA

ARTICLE INFO

Article history:
Received 6 October 2010
Received in revised form
18 January 2011
Accepted 23 January 2011
Available online 1 February 2011

Keywords:
Monte Carlo methods
Hypersonic flow
Planetary entry
Hypersonic plasma radiation
Random number database
Line-by-line radiation

ABSTRACT

A new databasing scheme is developed for Monte Carlo Ray Tracing methods applied to hypersonic planetary entry. In this scheme, the complex relationships for the emission wavelength selection of atomic and molecular species in nonequilibrium flows are simplified by developing random number relationships for individual transitions, as opposed to using relationships for the spectral emission coefficient of a given species. These new techniques speed up wavelength selection by about 2 orders of magnitude, and offer flexibility for use in weighted or part-spectrum Monte Carlo solvers.

1. Introduction

The Monte Carlo Ray Tracing (MCRT) method is an attractive method for the solution of the Radiative Transfer Equation (RTE) because it can be applied to relatively difficult problems without large increases in coding complexity or cost. In thermal radiation most MCRT methods are applied as direct methods, that is statistically (and physically) meaningful rays are traced through a domain. The method has been applied to radiative heat transfer problems since the 1960s, being first developed by Fleck [1,2] and Howell and Perlmutter [3,4]. Reviews of the method were presented by Howell in a monograph [5], and later in [6]. MCRT simulations have also been combined with stochastic particle tracking solvers [7,8] in fully coupled turbulent combustion simulations. Recently, MCRT solvers have been applied to hypersonic entry problems, incorporating it into a direct simulation Monte Carlo flow solver [9], and to continuum applications [10]. One of the challenges of modeling radiation in hypersonic flows is the strong spectral variation of radiative properties, and their dependencies on a large number of parameters (several unique temperatures, and the number densities of electrons, ions, and heavy particles). For atomic species, the strength of emission and absorption of bound–bound, bound-free, and free–free transitions in nonequilibrium conditions depends on the number of atoms in the associated electronic states, which can be computed following the Quasi-Steady State (QSS) approximation, with dependencies of electron temperature (T_e) the ratio of ions to atoms (n_+/n_s) and the number density of electrons (n_e), resulting in spectral absorption and emission coefficients with dependencies on translational temperature, electronic temperature, number density of ions, number density of electrons and number density of atoms (T_t,T_e,n_+,n_e,n_s) and wavelength (λ) [11,12]. For molecular species the spectral emission and absorption coefficient depend on 7 primary variables, namely ($T_t,T_e,T_r,T_v,n_e,n_a,n_m;\lambda$) where T_r is the rotational temperature, T_v is the vibrational temperature, n_a is the

* Corresponding author. Tel.: +1 209 228 4113.
E-mail address: mmodest@ucmerced.edu (M.F. Modest).

0022-4073/$ - see front matter © 2011 Elsevier Ltd. All rights reserved.
doi:10.1016/j.jqsrt.2011.01.028

Nomenclature

E	photon bundle energy, W
I_λ	spectral intensity, W/m^2 Å sr
n	number density, m^{-3}
n_a	number density of atomic species, m^{-3}
n_e	number density of free electrons, m^{-3}
$n_{e'}$	upper electronic state population, m^{-3}
$n_{e''}$	lower electronic state population, m^{-3}
$n_{l'}$	upper ro-vibrational state population for molecular bound–bound line l, m^{-3}
n_m	number density of molecules, m^{-3}
n_+	number density of ions, m^{-3}
N_s	total number of species, –
Q_{vJ}	ro-vibrational partition function
$\nabla \cdot \mathbf{q}_r$	divergence of radiative heat flux, W/m^3
s	distance along path, m
T_t	translational temperature, K
T_r	rotational temperature, K
T_v	vibrational temperature, K
T_e	free electron temperature, K

Greek letters

ε_λ	emission coefficient, W/m^{-3} Å sr
ε	total emission, W/m^{-3} sr
κ_λ	absorption coefficient, m^{-1}

Subscripts

d	electronic system index
D	Doppler line width
e	electronic state index
i,s	species index
J	rotational state index
l	transition index
p	transition type index
q	narrow band index
v	vibrational state index
V	Voigt line width
λ	at a given wavelength, or per unit wavelength

Superscripts

bb	bound–bound
bf	bound-free
ff	free–free
$*$	cross-sectional or functional
$'$	upper state
$''$	lower state

number density of atoms, and n_m is the number density of molecules. Ozawa et al. [13] were the first todevelop a property databasing technique for use with Monte Carlo solvers in hypersonic problems, to the author's knowledge. While the database of Ozawa et al. [13] made line-by-line (LBL) accurate Monte Carlo solutions in Earth entry possible, the calculation of spectral properties remained the most expensive component when used in conjunction with ray tracing methods [10]. The goal of this paper is to outline methods to reduce the computational time for emission wavelength selection for use in general Monte Carlo ray tracing solvers, to make solutions tractable in hypersonic flow solvers.

2. Numerical method

The RTE for nonequilibrium hypersonic flowfields in the absence of scattering may be written as

$$\frac{dI_\lambda}{ds} = \mathbf{s} \cdot \nabla I_\lambda = \varepsilon_\lambda - \kappa_\lambda I_\lambda \tag{1}$$

where I_λ is the local spectral intensity, ε_λ is the (nonequilibrium) emission coefficient, and κ_λ is the absorption coefficient. In the photon Monte Carlo method the RTE is solved by tracing statistical photon bundles. Bundles are emitted into random directions at random wavelengths from random locations in each cell in the computational domain, and the sum of emitted energy carried by all bundles from a cell must conserve emission energy. So-called random number relations must be developed to obtain statistically meaningful locations, directions and wavelengths of emitted bundles, as explained in detail in Modest [14]. For wavelength selection, the random number is chosen following the cumulative distribution function such that the fraction of energy emitted below a given wavelength is equal to a random number (0,1] R_λ, or

$$R_\lambda = \frac{\int_0^\lambda \varepsilon_\lambda \, d\lambda}{\int_0^\infty \varepsilon_\lambda \, d\lambda} \tag{2}$$

where ε_λ is the emission coefficient for the cell, which is the sum over all emitting species in the flow,

$$\varepsilon_\lambda = \sum_{s=1}^{n_s} \varepsilon_{s\lambda} \tag{3}$$

In hypersonic flows there are several types of quantum transitions, which accompany emission and absorption events. For atomic species there are bound–bound electronic transitions, in which an electron transitions to a new bound state by release or capture of a photon at a specific discrete wavelength, bound-free transitions where an electron enters into or exits from an atomic orbit leading to emission and absorption coefficients, which are continuous across the spectrum, and free–free transitions, where a passing electron is slowed by the atomic field, again yielding a continuous spectrum. In the model for emission wavelength selection described in Ozawa et al. [13], all bundles carry the same energy. First, a random number for emission wavelength, R_λ is drawn, in an n_s species system, and the emitting species s is found according to

$$s = j \quad \text{if} \quad \frac{\sum_{i=1}^{j-1} \varepsilon_i}{\sum_{i=1}^{n_s} \varepsilon_i} < R_\lambda < \frac{\sum_{i=1}^{j} \varepsilon_i}{\sum_{i=1}^{n_s} \varepsilon_i} \tag{4}$$

where ε_i is total emission by species i in the given cell, i.e.

$$\varepsilon_i = \int_0^\infty \varepsilon_{i\lambda}\, d\lambda \tag{5}$$

Once the emitting species is found, R_λ is rescaled according to

$$0 \le R_{s\lambda} = \frac{R_\lambda \sum_{i=1}^{n_s} \varepsilon_i - \sum_{i=1}^{j-1} \varepsilon_i}{\varepsilon_j} \le 1 \tag{6}$$

This rescaled random number, $R_{s\lambda}$, selects photons of equal strength from species s, with wavelength found from a probability density function defined by

$$R_{s\lambda} = \frac{\int_0^\lambda \varepsilon_{s\lambda}\, d\lambda}{\varepsilon_s} \tag{7}$$

For atomic species, the calculation of Eq. (7) includes contributions from all lines ($O(100)$) of species s, in addition to continuum emission from bound-free and free–free transitions. For molecular species, the calculation of Eq. (7) involves contributions from all lines ($O(10000)$) of that species. In order to make this process efficient, Ozawa et al. [13] carried out the evaluation of Eq. (7) in two steps. First an approximate λ is found using a precalculated database, which contains precalculated values of $\int_0^\lambda \varepsilon_{s\lambda} d\lambda / \int_0^\infty \varepsilon_{s\lambda}\, d\lambda$ as a function of $\lambda, T_e, n_e/n_s$ and n_+/n_s for atomic species, and for molecular species as a function of λ, T_r and T_v. Once an approximate λ is found, the line shapes of all lines in the vicinity of the approximate λ and continuum contribution are added. To determine the exact value for λ a bisection search is then conducted, with Eq. (7) evaluated at two surrounding wavelengths, and the search is refined to a wavelength interval of 0.005 Å, at which point linear interpolation is performed to return a final λ. This bisectional search is computationally expensive, because many property evaluations are required. In addition, this method requires that all photons carry equal energy.

In the scheme of Ozawa et al. [13] the concept of superposition of emission coefficients is used to allow for separation of species, i.e., overlap between species need not be considered for emission. Under the scheme presented here the property of superposition of emission is utilized more extensively, recognizing that overlap of individual lines within a species also need not be considered. Rather than choosing an approximate location for λ and considering the overlap of neighboring lines and continuum radiation, all lines and all continuum transitions are separated. For atoms Eqs. ((4) and (6)) are used two more times, first to select the type of transition (bound–bound, bound-free, free–free) and a finally time to select a particular transition (e.g., a particular bound–bound line). Fig. 1 shows a sample selection tree, where the emitting species is first selected based on the proportion of energy contribution to total emission. As each molecular species may have many electronic systems, all molecular emission is grouped by electronic systems and each is considered as an independent "species", then a narrow-band is selected, then an individual molecular line. Once the individual transition is selected, and R_λ is rescaled the final time, the wavelength is selected from within the chosen transition. Following Eqs. ((4) and (6)), transition selection and rescaling requires knowledge of

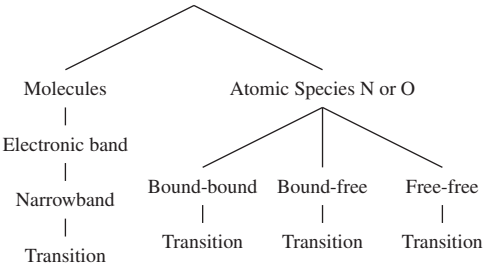

Fig. 1. Transition selection structure.

the total integrated emission from a transition (ε_l^p), which must be calculated efficiently. Once a given transition is selected, quick evaluation of λ ($R_{l\lambda}^p$) via Eq. (7) must be performed for that particular transition. Since, for Earth entry applications, 95% or more of emitted energy comes from atomic species, atomic species relationships will be the primary focus of this work.

2.1. Atomic bound–bound lines

The absorption coefficient at wavelength λ for a specific bound–bound transition is given by [15]

$$\kappa_\lambda^{bb} = \kappa_l^c (n_{e''} - n_{e'}) \phi_\lambda \tag{8}$$

with corresponding emission coefficient of

$$\varepsilon_\lambda^{bb} = \varepsilon_l^c n_{e'} \phi_\lambda \tag{9}$$

where $n_{e'}$ is the upper level electronic state population, $n_{e''}$ is the lower level electronic state population and ϕ_λ is the normalized line shape for a given line. The Voigt line shape is assumed for ϕ_λ, as atomic lines are subject to both Doppler and Stark broadening, where Stark broadening is assumed to follow the Lorentz line shape. The line center constants (κ_l^c) used in this work are from NIST [16], and have been grouped and assembled by Johnston et al. [17–19]. The Approximate Atomic Collisional-Radiative (AACR) model of Johnston et al. [19] is used for the QSS calculation, to determine the electronic state populations for each level. The total emission for a single line l is simply

$$\varepsilon_l^{bb} = \varepsilon_l^c n_{e'} \tag{10}$$

and the random number relationship for a single line l is then

$$R_\lambda^{bb} = \frac{\int_0^\lambda \varepsilon_l^{bb} \phi_\lambda\, d\lambda}{\varepsilon_l^{bb}} = \int_0^\lambda \phi_\lambda\, d\lambda \tag{11}$$

The total emission for all lines can be calculated once and for all at the beginning of each Monte Carlo calculation, and Eqs. ((4) and (6)) are used to select a line, and rescale the random number. Since most of atomic emission comes from very few ($O(10)$) very strong lines, search time can be greatly reduced by sorting the lines according to emission line strength, and selecting lines from the sorted table. The partially integrated Voigt line shape can be expressed as a function of normalized wavelength, and

ratio of Doppler to Voigt line widths [20], i.e.,

$$\phi_\lambda = \phi_\lambda\left(\frac{|\lambda-\lambda_c|}{w_V}, \frac{w_D}{w_V}\right) \tag{12}$$

where, w_D is the Doppler line width, and w_V is the Voigt line width. The line shape is always considered to be symmetric about the line center, and

$$\int_0^{\Delta\lambda} \phi_\lambda d\Delta\lambda = \Phi\left(\frac{\Delta\lambda}{w_V}, \frac{w_L}{w_V}\right) \quad \text{where} \quad \int_0^{\infty} \phi_\lambda d\Delta\lambda = 0.5 \tag{13}$$

with $\Delta\lambda$ measured from the line center. It is sufficient to database only one-half of the line with the sign of the rescaled random number

$$R_{l\lambda}^{*bb} = R_{l\lambda}^{bb} - 0.5 \tag{14}$$

determining the direction of the offset from the line center.

The function Φ is then inverted and tabulated so that

$$\frac{\Delta\lambda}{w_V} = \mathrm{sgn}(R_{l\lambda}^{*bb})\Phi^{-1}\left(|R_{l\lambda}^{*bb}|, \frac{w_L}{w_V}\right) \tag{15}$$

This function is currently stored using 51 points for w_L/w_V [0,1], and 201 points for R_λ from [0,0.5]. The points in R_λ space are distributed according to

$$R_i = \arctan(10^{-5+(i-1)/20})/\pi \quad \text{for } i = 1,\ldots,201$$

which is based on the integrated Lorentz shape, to reduce the required number of points to accurately capture the line shape distribution. Double linear interpolation is used to evaluate Φ^{-1}.

2.2. Atomic bound-free transitions

In the case of bound-free transitions, the wavelength of transition is defined by the kinetic energy of the free electron E_k, or,

$$\lambda = \frac{hc}{E_\infty - E_e + E_k}, \quad \lambda(E_{kmax}) \le \lambda < \lambda(E_{kmin}) \tag{16}$$

where E_∞ is the ionization potential of the atom, and E_e is the energy of the e-th bound level associated with transition l. The electron energy is described by a continuous Maxwellian distribution, resulting in a wavelength distribution which is also continuous. While the wavelength distribution for each of the 35 N transitions and 16 O transitions is continuous, it is still desirable to use the same scheme as in Section 2.1 for wavelength selection, that is to select a transition first based on the total emitted energy of that transition l and then select a wavelength based on a random number relationship for a given transition l. In order to make this process efficient, the total energy (ε_l^{bf}) and random number–wavelength relationship ($\lambda_l(R_{l\lambda}^{bf})$) can be databased.

The absorption coefficient for a bound-free transition is defined [18] as

$$\kappa_{l\lambda}^{bf} = \kappa_{l\lambda}^{*bf}(n_{e''} - n_{e'}) \tag{17}$$

where $\kappa_{l\lambda}^{*bf}$ is the bound-free absorption cross-section for a given bound-free transition l, which is purely a function of wavelength for each transition and is easily tabulated for each transition. An emission cross-section can be written as

$$\varepsilon_{l\lambda}^{*bf} = \kappa_{l\lambda}^{*bf} I_{b\lambda}^{bf} \tag{18}$$

where the bound-free Planck function $I_{b\lambda}^{bf}$ is the equilibrium Planck function evaluated at the free electron temperature. The emission coefficient can be found from

$$\varepsilon_{l\lambda}^{bf} = \varepsilon_{l\lambda}^{*bf} n_{eE} \tag{19}$$

where n_{eE} is the population of the electronic state associated with bound-free transition e in equilibrium with electrons at electron temperature T_e, and is given by the Saha-Boltzmann equation [19]. In order to apply Kirchoff's law, chemical equilibrium is assumed to exist among the atoms, ions, and electrons.

As in the case of bound–bound lines, bound-free transition selection requires efficient calculation of the total energy from transition l,

$$\varepsilon_l^{bf} = \int_{\Delta\lambda l} \varepsilon_{l\lambda}^{bf} d\lambda = \varepsilon_l^{*bf} n_{eE}. \tag{20}$$

The wavelength-integrated emission cross-section, ε_l^{*bf} is a function of T_e only, which can be easily tabulated. $\varepsilon_l^{bf*}(T_e)$ is precalculated and stored in 500 K increments from 500 to 30,000 K. Evaluation of ε_l^{bf} for each band (35 for N, and 17 for O) involves one linear interpolation and one multiplication; ε_l^{bf} can be precalculated for each cell and ordered to reduce search time. In addition the function

$$R_{l\lambda}^{bf} = \frac{\int_0^\lambda \varepsilon_{l\lambda}^{bf}}{\varepsilon_l^{bf}} = \frac{\int_0^\lambda \varepsilon_{l\lambda}^{*bf}}{\varepsilon_l^{*bf}} \tag{21}$$

for each transition is a function of λ and T_e only. Thus $R_\lambda(\lambda,T_e)$ can be evaluated and inverted, leading to

$$\lambda = \lambda_l(R_{l\lambda}^{bf}, T_e) \tag{22}$$

Again, this function is tabulated and stored for each bound-free transition. Currently, the random number database includes electron temperatures ranging from 500 to 30,000 K with 61 datapoints, and R_λ varies from 0 to 1 with 101 points, with linear spacing. Double linear interpolation is used to calculate the emission wavelength for a given bound-free transition.

2.3. Atomic free–free transitions

The absorption coefficient for free–free transitions is defined as [12]

$$\kappa_\lambda^{ff} = n_+ n_e \kappa_\lambda^{*ff} \tag{23}$$

where the free–free absorption function κ_λ^{*ff} is a function of electron temperature and wavelength [12], and has been tabulated in a two-dimensional array. Since there are no bound states, there is just one continuous transition modeled for each atomic species

The emission function is calculated using the Planck function at the electron temperature [12], following the assumption that the energy distribution of the free

electrons is Maxwellian, leading to,

$$\varepsilon_\lambda^{*ff} = \kappa_\lambda^{*ff} I_{b\lambda}^{ff} \tag{24}$$

Since κ_λ^{*ff} is a function of electron temperature and wavelength, and the Planck function is a function of electron temperature and wavelength, then the wavelength integrated total emission function $\varepsilon^{*ff} = \varepsilon^{ff}/n_+ n_e$ is also a function of electron temperature only, and can be calculated as a function of T_e. Similarly, the random number relationship is a function of electron temperature and wavelength;

$$R_\lambda^{ff}(\lambda, T_e) = \frac{\int_0^\lambda \varepsilon_\lambda^{*ff}}{\varepsilon^{*ff}} \tag{25}$$

$R_\lambda^{ff}(\lambda, T_e)$ can be evaluated and inverted, leading to

$$\lambda = \lambda(R_\lambda^{ff}, T_e) \tag{26}$$

This function is tabulated and stored for each free–free transition. Currently, the random number database ranges in T_e from 500 to 30,000 K with 61 datapoints, and R_λ^{ff} varies from 0, 1 with 101 points, with one database required for each species. Again, double linear interpolation is used to evaluate the function between abscissae.

2.4. Molecular transitions

The molecular species considered in this work are the same as those employed by Sohn et al. [12] Molecular emission and absorption data are stored by individual electronic systems. Therefore, the transition selection process, shown if Fig. 1, involves selection of an atomic species or all molecules, then the electronic system, without an intermediate selection of the emitting species. The emission coefficient for a particular band can be found from [12]

$$\varepsilon_\lambda^d = \sum_{l=1}^{N_d} \varepsilon_l^{cd} \phi_{dl\lambda} \tag{27}$$

where l is the line index, d is the electronic system index ε_l^{cd} is a constant for line l in band d, and $\phi_{dl\lambda}$ is the line shape for line l. The line shape for all molecular lines is taken to be Doppler, as Stark broadening for molecular species is small, and pressures are low enough that collision broadening can be neglected. Following the same logic used in atomic bound–bound wavelength selection, line transitions are selected without considering line overlap. The emission line strength (ε_l^d) for a line in a given electronic system (d) is

$$\varepsilon_l^d = \varepsilon_l^{cd} n_{l'} \tag{28}$$

where $n_{l'}$ is the upper state population, which is different for each line in the band, i.e.;

$$n_{l'} = \frac{n_{e'}}{Q_{v'J'}}(2J'+1)\exp\left[-\frac{hc}{k}\left(\frac{E(v')}{T_v} + \frac{E(J')}{T_r}\right)\right] \tag{29}$$

where $n_{e'}$ is the electronic upper state population, which can be determined via the quasi-steady state approximation as a function of $(T_t, T_e, T_r, T_v, n_e, n_a, n_m)$, and is a constant for the entire band, $Q_{v'J'}$ is a function of (T_r, T_v) the upper state total partition function which is also constant over the electronic system, J' is the rotational quantum number, v' is the vibrational quantum number, $E(v')$ is the state vibrational term energy, and $E(J')$ is state rotational term energy. While $n_{e'}$ is a function of 6 primary variables $(T_t, T_e, T_r, T_v, n_e, n_a, n_m)$, $n_{e'}$ and $Q_{v'J'}$ are constants for each molecular band, and can be factored out to reduce the number of dependencies required in the database, in a method similar to Ozawa et al. [13] The wavelength-integrated emission from ε^{*d} is a function of T_r and T_v only, where

$$\varepsilon^{*d}(T_v, T_r) = \frac{\varepsilon^d(T_v, T_r)}{n_{e'}/Q_{v'J'}} = \frac{\sum_{l=1}^{n} \varepsilon_l^{cd} n_{l'}}{n_{e'}/Q_{v'J'}} \tag{30}$$

Because there are many rovibrational transitions in each electronic system, it is not practical to precalculate the line strength for each individual line. It is desired then to precalculate the line strengths of groups of lines, to reduce the required searching effort. This is done on a wavelength basis, i.e.,

$$\varepsilon_q^{*d}(T_v, T_r) = \frac{\sum_{l=j_1(q)}^{j_2(q)} \varepsilon_l^{cd} n_{l'}}{n_{e'}/Q_{v'J'}} \tag{31}$$

where $j_2(q)$ represents the maximum line index for a given narrow band q, and $j_1(q) = j_2(q-1)+1$. $\varepsilon_{d\lambda}^*(T_v, T_r)$ and $j_2(q)$ are stored in wavelength intervals of 5 Å. Once a group of lines is selected, the individual line strengths are calculated on the fly for lines $j_1(q)$ to j_2, and the proper line is selected from the narrow band using the rescaled random number. After line selection has taken place, linear interpolation from the function $\Phi^{-1}(R_\lambda^{bb}, 0)$ is performed, as the line shape is assumed to be Doppler for molecular transitions. The Doppler profile is used as collision broadening in atmospheric entries is small. Predissociative broadening is not considered in this work, but could be adopted by considering the same Voigt profile used for atomic transitions.

3. Verification and sample calculations

Sample calculations are performed to assess the accuracy and efficiency of the computational method. The accuracy of the method is investigated by comparing the emission wavelength selection to LBL calculations at an arbitrary cell condition, representative of a highly nonequilibrium region of a shock layer in Earth entry conditions, shown in Table 1.

3.1. Verification

The spectral dependencies of the Monte Carlo method are evaluated using a binning method. The total energy (E_{tot}) for the given cell is calculated and a bundle energy of $E_{bundle} = E_{tot}/n$ is assigned to each bundle, where n is the number of bundles emitted from the cell for a calculation. A wavelength is then selected, and the amount of energy is deposited into a wavelength bin of step size $\Delta\lambda$. This was done for atomic bound–bound, bound-free, free–free and molecular emission separately, as the large differences in emitted energies for each type of transition can prevent a proper number of samples from being selected

Table 1
Conditions for sample spectral calculations.

Energy mode	Temperature (K)
T	19,448
T_V	11,246
T_R	7714
T_e	11,246
Species	Number density (cm^{-3})
N_2^+	1.66×10^{13}
N_2	1.77×10^{16}
NO	1.06×10^{15}
O_2	1.79×10^{15}
N	1.39×10^{16}
O	8.18×10^{15}
N^+	6.59×10^{15}
O^+	1.84×10^{15}
e^-	8.60×10^{15}

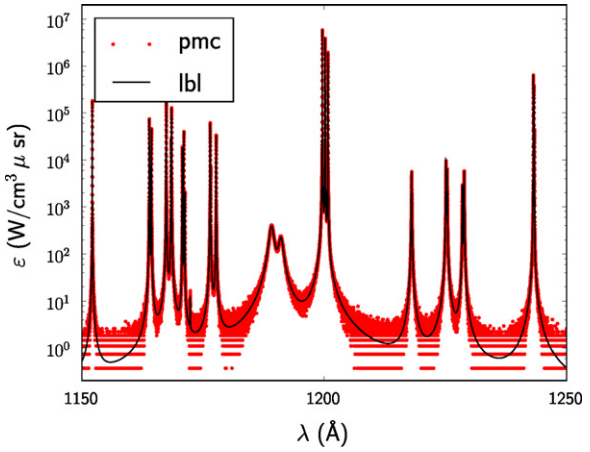

Fig. 2. Comparison of atomic bound–bound emission from LBL calculation and current databasing scheme.

for lower emission energy transitions. Calculations for atomic bound–bound transitions of both N and O were carried out using 1 billion bundles with a bin step size $\Delta\lambda = 0.005$ Å, requiring a calculation time of 550 s on a 2.8 GHz Pentium QuadCore machine. The same calculations using the scheme of Ozawa et al. [13] takes 12,000 s, or about 20 times longer. Fig. 2 indicates that all of the lines are selected properly, while a zoom-in at the spectral region of 1199–1201 Å (Fig. 3) demonstrates that line shape including complex overlap of lines from different species is captured well. For stronger emission regions near line centers there are many samples, and the behavior is captured exactly. For lower emission regions near the line wings there are not as many samples, but spectral behavior is captured correctly on average.

Calculations for molecular line radiation show similar results, as demonstrated in Fig. 4 for a small part of the NO band. Computational time for molecular species (1 billion bundles) is 1600 s, compared to 120,000 s using the scheme of Ozawa et al. [13], again showing improvement in computational time by a factor of 70.

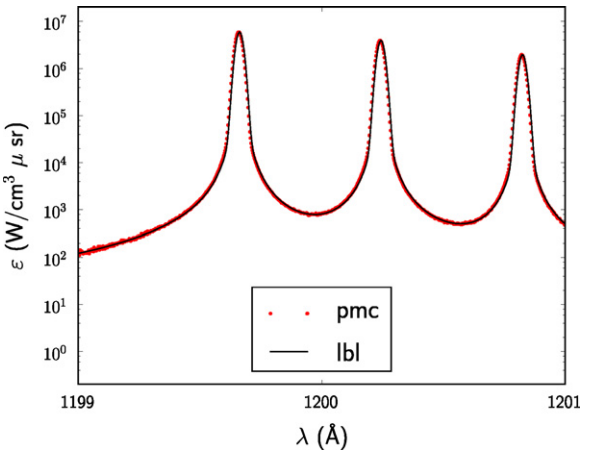

Fig. 3. Comparison of atomic bound–bound emission from LBL calculation and current databasing scheme (zoom).

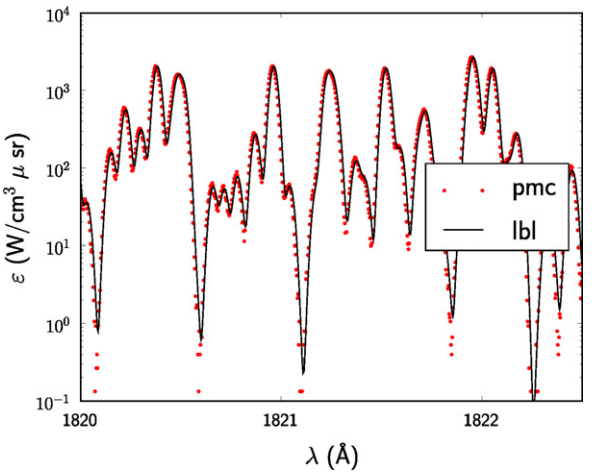

Fig. 4. Comparison of molecular (NO) emission from LBL calculation and current databasing scheme (zoom).

Calculations for atomic bound-free and free–free transitions of both N and O were also carried out using 1 billion bundles, this time with a bin step size $\Delta\lambda = 0.5$ Å, for bound-free and a bin size of $\Delta\lambda = 2$ Å for free–free. For bound-free emission 240 s were required and 213 s for free–free emission. Fig. 5 shows the spectral variations of bound-free emission for the cell conditions given in Table 1. Agreement between the Monte Carlo method and the LBL calculation using the data from Johnston et al. [18] is excellent in the high emission spectral regions, and is captured correctly on average in low emission regions. Free–free spectral data are plotted in Fig. 6, also showing good agreement.

3.2. Sample stagnation line calculation

A sample 1-D calculation was then performed using the stagnation line of the CEV from Feldick et al. [21], and compared with LBL results. In this calculation there are 148 cells, with a total of 10 million bundles traced, and all species and transitions in the database are considered. Fig. 7

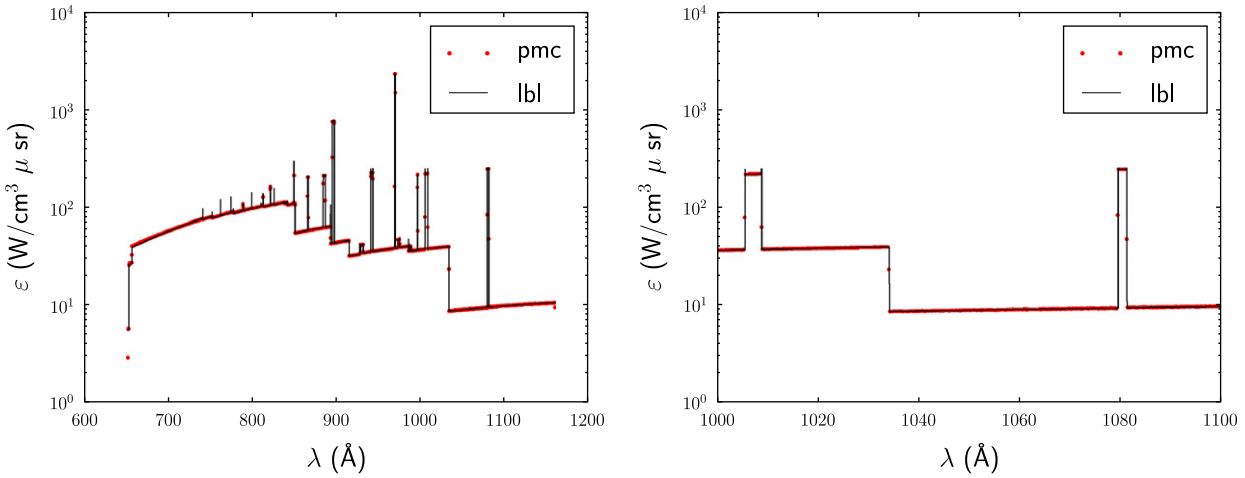

Fig. 5. Comparison of atomic bound-free emission from LBL database of calculation and current databasing scheme.

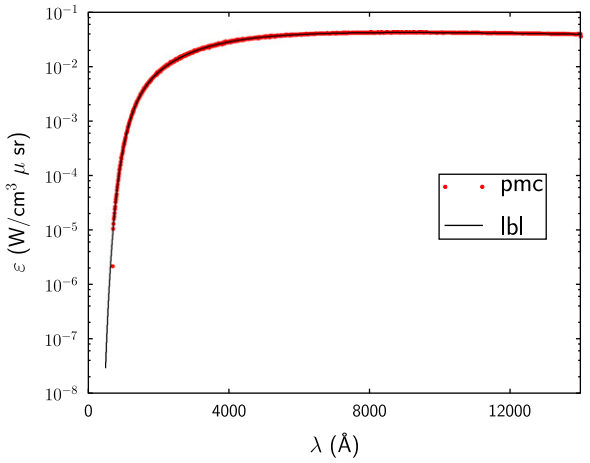

Fig. 6. Comparison of atomic free–free emission from LBL database of calculation and current databasing scheme.

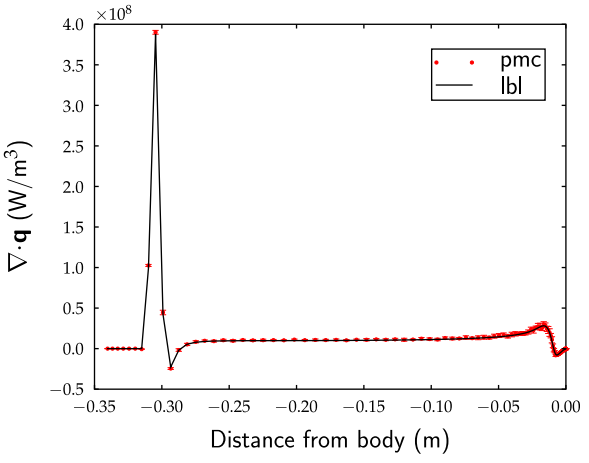

Fig. 7. Comparison of molecular emission from LBL calculation and current databasing scheme.

shows that the Monte Carlo solver captures line-by-line results to statistical accuracy, denoted by the error bars which represent one standard variation of the mean.

In a Monte Carlo simulation of radiative transfer there are three major calculations, which contribute to the computational cost of the solution: the initial setup (calculation of QSS, total cell emission, and total emission of each transition), which is done once per cell, then tracing, which involves emission wavelength selection performed several times per cell, and finally evaluation of the absorption coefficients, which is required for each photon's wavelength in multiple cells. The initial setup cost is minimal for both the solver used here, and for that of Ozawa et al. For the method developed here, tracing 10 million bundles requires 7100 cpu seconds, which is about 10 times faster than that of our previous spectral solver [10], using the database of Ozawa et al [13]. The emission wavelength selection is about 20 times faster than Ozawa et al., as the emission is predominantly due to atomic line emission. The calculation time of the absorption coefficients has also been reduced through methods not presented here.

4. Conclusions

A new wavelength selection scheme for Monte Carlo ray tracing solvers applied to hypersonic flows was developed, to increase flexibility and to reduce computational cost. The scheme is based on the idea of superposition of emission to select individual transitions. This allows wavelengths to be calculated from precomputed tables, eliminating the need for expensive searching. Computational time is about 2 orders of magnitude faster for emission wavelength selection than with our previous database. When applied to a sample flowfield, LBL accurate results are produced with a time savings factor of about 10 compared to our previous solver.

Acknowledgments

The authors gratefully recognize support from NASA grant NNXO7AC47A.

References

[1] Fleck JA. The calculation of nonlinear radiation transport by a Monte Carlo method. Technical Report UCRL-7838, Lawrence Radiation Laboratory; 1961.
[2] Fleck JA. The calculation of nonlinear radiation transport by a monte carlo method: statistical physics. Methods Comput Phys 1961;1:43–65.
[3] Howell JR, Perlmutter M. Monte Carlo solution of thermal transfer through radiant media between Gray walls. ASME J Heat Transfer 1964;86(1):116–22.
[4] Howell JR, Perlmutter M. Monte Carlo solution of thermal transfer in a nongrey nonisothermal gas with temperature dependent properties. AIChE J 1964;10(4):562–7.
[5] Howell JR. Application of Monte Carlo to heat transfer problems. In: Hartnett JP, Irvine TF, editors. Advances in heat transfer, vol. 5. New York: Academic Press; 1968.
[6] Howell JR. The Monte Carlo method in radiative heat transfer. ASME J Heat Transfer 1998;120(3):547–60.
[7] Wang A, Modest MF, Haworth DC, Wang L. Monte Carlo simulation of radiative heat transfer and turbulence interactions in methane/air jet flames. J Quant Spectrosc Radiat Transfer 2008;109(2):269–79.
[8] Mehta RS, Wang A, Modest MF, Haworth DC. Modeling of turbulent ethylene/air jet flames using hybrid finite volume/Monte Carlo methods. In: CHT-08 advances in computational heat transfer. Begell House Inc.; 2008.
[9] Ozawa T, Wang A, Levin DA, Modest MF. Development of a coupled DSMC—particle photon Monte Carlo method for simulating atomic radiation in hypersonic reentry flows. J Thermophys Heat Transfer 2010;24(3):612–22.
[10] Feldick AM, Giegel J, Modest MF. A spectrally accurate tightly-coupled 2-D axisymmetric photon Monte-Carlo RTE solver for hypersonic entry flows. In: ASME summer heat transfer conference, San Francisco, California, Paper no. HT2009-88241; July 2009.
[11] Lamet J-M, Babou Y, Rivière P, Perrin M-U, Soufiani A. Radiative transfer in gases under thermal and chemical nonequilibrium conditions: application to earth atmospheric re-entry. J Quant Spectrosc Radiat Transfer 2008;109(2):235–44.
[12] Sohn I, Bansal A, Levin DA, Modest MF. Advanced radiation calculations of hypersonic reentry flows using efficient databasing schemes. J Thermophys Heat Transfer 2010;24(3):623–37.
[13] Ozawa T, Modest MF, Levin DA. Spectral module for photon Monte Carlo calculations in hypersonic nonequilibrium radiation. ASME J Heat Transfer 2010:023406-1–8.
[14] Modest MF. Radiative heat transfer. 2nd ed. New York: Academic Press; 2003.
[15] Park C. Nonequilibrium hypersonic aerothermodynamics. New York: Wiley; 1990.
[16] Ralchenko Y, Kramida A, Reader J. NIST ASD team. NIST Atomic Spectra Database, Version 3.1.0; July 2006.
[17] Johnston CO, Hollis BR, Sutton K. Radiative heating methodology for the huygens probe. AIAA Paper no. 2006-3426 2006. In: Ninth AIAA/ASME joint thermophysics and heat transfer conference, San Francisco, California, 2006.
[18] Johnston CO, Hollis BR, Sutton K. Spectrum modeling for air shock-layer radiation at lunar-return conditions. J Spacecr Rockets 2008;45(5):865–78.
[19] Johnston CO, Hollis BR, Sutton K. Non-Boltzmann modeling for air shock-layer radiation at lunar-return conditions. J Spacecr Rockets 2008;45(5):879–90.
[20] Arnold JO, Whiting EE, Lyle GC. Line by line calculation of spectra from diatomic molecules and atoms assuming a Voigt line profile. J Quant Spectrosc Radiat Transfer 1969;9:775–98.
[21] Feldick AM, Modest MF, Levin DA. Closely coupled flowfield-radiation interactions during hypersonic reentry. J Thermophys Heat Transfe, in press.